Superparamagnetic Composite of Magnetite-CTAB as an Efficient Adsorbent for Methyl Orange

Nor Harisah, Dwi Siswanta, Mudasir Mudasir, and Suyanta Suyanta*

Department of Chemistry, Faculty of Mathematics and Natural Sciences, Universitas Gadjah Mada, Sekip Utara, Yogyakarta 55281, Indonesia

*** Corresponding author:**

tel: +62-8568936689
email: suyanta_mipa@ugm.ac.id

Received: October 1, 2021
Accepted: January 4, 2022

DOI: 10.22146/ijc.69499

Abstract: *In this study, a superparamagnetic composite of magnetite-cetyltrimethylammonium bromide (CTAB) has been prepared by the coprecipitation method and then applied as a charge-selective adsorbent of anionic methyl orange (MO). The VSM (Vibrating Sample Magnetometer) measurement suggests the superparamagnetic property of MNPs (Magnetite Nano Particles) with a magnetic saturation of 49.2 emu g^{-1}. The SEM image exhibits the significant difference in particle size from nanometers in uncoated magnetite to micrometers in magnetite-CTAB. Calculations with ImageJ software indicate that the diameter of the composite is in the range of 2–13 μm, with an average diameter of 6.56 μm, possibly consisting of hundreds to thousands of magnetite-CTAB micelles. The adsorption kinetics of MO over magnetite-CTAB follows the pseudo-second-order adsorption model of Ho and McKay with a rate constant (k_2) of 3.54 × 10^3 g mol^{-1} min. The adsorption isotherm is well described by the Langmuir model with a Langmuir constant (K_L) of 7.46 × 10^4 L mol and a maximum capacity (q_m) of 27.9 mg g^{-1}. The developed material is intriguing because it can be easily and quickly recovered using an external magnet after adsorption and selectively adsorbs anionic dyes.*

Keywords: *superparamagnetic; composite; magnetite-CTAB; adsorption; methyl orange*

■ INTRODUCTION

Dyes are one of the primary sources of environmental contamination. The total amount of dyes used worldwide is estimated at over 10^7 kg per year, mainly originating from the textile industry [1]. Textile fibers have polar groups that can form a dipole-dipole bond with auxotrophic groups on dyes that are also polar [2]. Dyes are readily soluble in organic solvents or water, so they are difficult to remove by various physical, chemical, and biological methods [3]. The main problem with using reactive dyes in textiles is that not all of these dyes are adsorbed by the fabrics because the binding efficiency of fibers to the dyes is only 60–90%. The dyes that are not absorbed by the fibers are released into the environment and become hazardous waste [4].

Pollution of textile dyes in the water causes aesthetic damage, blocks light penetration, and interferes with the photosynthesis of aquatic plants, such as algae [5]. Textile dyes are also toxic, mutagenic, and carcinogenic [6-7]. Based on the charge of the dye molecule when ionized in water, two types of dyes can be mentioned, e.g., cationic and anionic dyes [8]. Due to its dangerous effect on the environment, several techniques for dye removal from water have been proposed. These include coagulation/flocculation, ozonization, oxidation, filtering with membrane, electrochemical processes, photocatalytic degradation, and adsorption [9]. Among those various techniques, adsorption normally becomes the choice because it is the most practical, simple, efficient, and economical way. Various types of adsorbents have been reported to be used for the adsorption of dyes, including zeolite, bentonite, sepiolite, smectite, mesoporous silica, orange peel, chitosan, alginate, and magnetite (Fe_3O_4) [1]. Although most of these materials are effective and efficient as adsorbents for the dyes, their handling after the

adsorption process becomes a serious problem because they are not easily recovered and separated from the pollutants. Therefore, a new adsorbent that can be easily separated and recovered, such as magnetite materials, should be developed.

It has been well known that superparamagnetic materials, such as magnetite nanoparticles (MNPs) with a particle size of less than 25 nm can be attracted by magnetic fields. Still, their magnetic properties will be lost when the magnet is removed [10]. This unique property makes it suitable to be used as a dye adsorbent. After the adsorption process, the adsorbent can be separated quickly by an external magnetic field, so it does not require centrifugation or filtration, which is usually required when other non-magnetite adsorbents are used. However, superparamagnetic materials such as MNPs synthesized in this study have limitations. For example, they tend to attract each other and agglomerate to form a bulk phase due to their magnetic properties. One strategy that can be used to prevent the formation of agglomeration is to trap the MNPs using surfactants as soon as they are formed so that their superparamagnetic property can be maintained. Cetyltrimethylammonium bromide (CTAB) is one of the most widely used cationic surfactants for such purposes. It will be ionized in water, resulting in cationic CTA^+ and anionic Br^-. The cationic CTA^+ will interact with the surface of magnetite to form a positive layer on the surface of magnetite so that it can be used to adsorb selectively anionic dyes.

It has been previously reported that the isoelectric point of magnetite is at around pH = 7 [11-12]. The synthesis of magnetite is generally carried out at a relatively high pH, i.e., pH = 11 [13], so its surface will be negatively charged. In the case of magnetite-CTAB preparation, spherical micelles in which the double-layered CTA^+ becomes a shell covering the MNPs core can be produced under these circumstances if an appropriate amount of CTAB is introduced into the MNPs sol [14]. The positive head of the CTA^+ polar groups in the first layer will face the center of the sphere containing MNPs and interact electrostatically with the negatively charged MNPs surface. Meanwhile, the hydrophobic groups of CTA^+ interact hydrophobically with other hydrophobic groups of CTA^+ positioned in the second layer [14]. The remaining polar groups of CTA^+ in the second layer are located on the surface of the spherical micelles, giving a positive charge to the double layer surface. Therefore, the material will adsorb anionic pollutants such as methyl orange (MO) by electrostatic interactions. So far, there have been extensive reports dealing with the synthesis and application of magnetite-CTAB composites [2-3,5-7]. However, to the best of our knowledge, there is still no work focusing on optimizing the CTAB mass in the synthesis. Yet, this parameter is crucial to be optimized to get the exact double-layer material with positively charged surfaces.

Furthermore, the application of these magnetite materials as charge-selective adsorbents of anionic dyes such as MO is also hardly reported, although the removal of MO by adsorption methods has been reported by many workers [10,15-18]. Chen et al. [10] have studied the kinetics and adsorption mechanism of methyl orange by surfactant modified *silkworm exuviae*. Protonated cross-linked chitosan has been used to adsorb MO [15], and the determination of biosorption conditions of MO by biomaterials of *humicola fuscoatra* has also been conducted [16]. The role of surface and pH on the adsorption behavior of MO onto wheat bran has been reported by Alzaydien [17], while an equilibrium, kinetic, and thermodynamic study of the removal of MO from aqueous solution via adsorption on cork as a natural and low-cost adsorbent has also been carried out [18]. None of the reported adsorbents used for this MO adsorption are magnetite materials.

Recently, Fisli et al. [19] have reported the synthesis of magnetite-CTAB and used the material for MO removal. However, the procedure used in this report did not control pH up to pH 11, did not optimize the mass of CTAB added, did not maintain the inert atmosphere, and used conventional mixing. As mentioned above, control of pH, as well as the amount of CTAB added to the reaction, are essential to get exactly a double layer with positively charged surfaces. Moreover, inert atmosphere control is also important to ensure that Fe^{2+} is not oxidized into Fe^{3+} during the

process. If this happens, magnetite will not be produced; instead, Fe_2O_3 will be obtained. In addition, conventional mixing by stirrer is also used in this report so that the reaction time is longer. In the present work, we introduce a new modified procedure for synthesizing magnetite-CTAB composite. The synthesis was done in the nitrogen atmosphere, and the addition of CTAB was optimized to get a double layer on the surface of magnetite so that the charge on the surface is positive. To speed up the reaction, ultrasonic mixing has also been used in the reaction. The obtained materials were characterized by FTIR, XRD, VSM, and SEM and then used for the adsorption of MO from aqueous samples. MO has been used as an anionic target in this study because it is extensively used in textile industries and is normally difficult to remove from water [1]. In the adsorption study, some parameters influencing the adsorption, including pH, contact time, and initial concentration, were optimized. Evaluation of kinetic adsorption was done by applying three types of kinetic models, e.g., Lagergren, Ho and Mckay, and Langmuir-Hinshelwood, while for isotherm adsorption, Langmuir and Freundlich were applied, and the recovery of the adsorbent using an external magnet was determined after adsorption. Meanwhile, Fisli et al. [19] used only one model for each parameter in the adsorption study of MO, i.e., the Ho and McKay kinetic model and the Langmuir isotherm model, and no recovery of adsorbent was conducted. Moreover, as the magnetite (MNP) is positioned deep in the core of the micelle, it is expected that it will be more protected from oxidation. As a result, the composites will have a long duration or high stability magnetic properties.

■ EXPERIMENTAL SECTION

Materials

The materials used in this study included CTAB (≥ 98% purity Merck, Germany), $FeSO_4{\cdot}7H_2O$ (≥ 99% purity Merck, Germany), $FeCl_3{\cdot}6H_2O$ (≥ 98% purity Merck, Germany), NH_4OH (27% purity Merck, Germany), MO (85% purity Merck, Germany), and methyl violet (MV, 75% purity Merck, Germany). The chemicals were used as purchased, and no further purification was performed. Distilled water was obtained from CV. Progo Mulyo Yogyakarta, Indonesia.

Instrumentation

The Bransonic 220 ultrasonic device was used as an ultrasonic beam source with a heating power of 100 W and a frequency of 48 kHz at 25–32 °C (room temperature). An X-ray diffractometer (XRD, Shimadzu XD-3H) was used to obtain the X-ray diffraction pattern, using $Cu_{K\alpha}$ powder irradiated at λ = 0.15418 nm. Shimadzu FTIR-8010PC was used for FTIR spectroscopic analysis, and the spectrum was recorded at a wavelength of 4000–400 cm^{-1} at room temperature using the KBr disc technique. A vibrating sample magnetometer (VSM Oxford 1.2H) was used to analyze the magnetic properties of the samples, using a magnetic field of up to 1.600 kA m^{-1} at room temperature. Scanning Electron Microscope (SEM, JEOL JSM-6510LA) was used to obtain the surface images of samples. The ImageJ software was used to process the obtained images. Spectrophotometer UV-Vis (Shimadzu UV-1700 E) was used to analyze the concentration of MO and MV at the λ_{max} of 464 nm and 582 nm, respectively.

Procedure

Synthesis of magnetite-CTAB

The new approach of magnetite-CTAB synthesis was developed by our groups here with the following procedure. Firstly, the nanocomposites of Magnetite-CTAB were synthesized by coprecipitation method, i.e., by adding NH_4OH (27%) solution dropwise into 100 mL of a solution containing $FeCl_3{\cdot}6H_2O$ (4.055 g), $FeSO_4{\cdot}7H_2O$ (2.085 g), and various masses of CTAB (0.365, 1.823, and 3.645 g) until the pH reached 11, and then the mixture was sonicated for 15 min. A flow of N_2 gas was continuously bubbled to the reactor to avoid oxidation by O_2 during the reaction. The precipitate was removed from the mixture by an external magnet, washed with distilled water to neutral pH, dried in an oven at 100 °C for 3 h, and stored in a desiccator. Each product was denoted as magnetite-CTAB-0.01, magnetite-CTAB-0.05, and magnetite-CTAB-0.10, respectively. A similar procedure but without CTAB was

used to synthesize the uncoated magnetite. All products were characterized by FTIR, XRD, and one product that gave the best performance during the preliminary test, e.g., magnetite-CTAB-0.10, was further characterized by SEM and VSM methods as an example.

Adsorption study

The determination of adsorption capacity as a preliminary test of different adsorbents was carried out by interacting the composite of magnetite-CTAB-0.01 (25 mg) with MO solution (10 mg L^{-1}, 20 mL) at pH 7. The mixture was then shaken for 2 h. The selection of pH 7 was based on the pH PZC of magnetite, which is around 7, so that the double layer of CTAB was maintained. After adsorption, the adsorbent was recovered using a magnetic bar, and the concentration of MO in the filtrate was analyzed by UV-Vis spectrophotometry at the λ_{max} of 464 nm. Next, similar experiments were carried out using magnetite-CTAB-0.05, magnetite-CTAB-0.10, and uncoated magnetite, respectively, as an adsorbent. To test the selectivity of the adsorbent towards anionic dyes, similar experiments using cationic MV were also carried out using the same adsorbents and the same procedure as used for MO, except that the spectrometric analysis of MV in the filtrate was done at the λ_{max} of 582 nm. The following Eq. (1) [20] was used to calculate the adsorption capacity of both MO and MV:

$$q_e = \frac{(C_o - C_t)V}{m} \quad (1)$$

in which q_e is the adsorption capacity (mg g^{-1}), C_o is the initial concentration (mg L^{-1}), C_t is the concentration at time t (mg L^{-1}), V is the volume of the solution (L), and m is the mass of the adsorbent (g).

Further experiments were the determination of optimum conditions for the adsorption MO, and it was done only to the adsorbent with the highest adsorption capacity of magnetite-CTAB. The effect of pH on the adsorption capacity was studied using the same experiments but with pH variations in the range 4–9. The adsorption kinetics was studied by doing the same experiments but with variations of contact time of 5, 10, 15, 30, 60, 90, 120, 150, 180, 210, 240, and 270 min at the optimum pH. The obtained data were evaluated using several kinetic models such as Lagergren, Ho-McKay, and Langmuir-Hinshelwood models. For the adsorption isotherms study, the same experiments were also done but with variations of dye concentration, namely 5, 10, 15, 20, 25, 30, 35, 40, 45, and 50 mg L^{-1} at the optimum pH and contact time. The data were evaluated using Langmuir and Freundlich Isotherms equations. The recovery test was carried out by separating the used adsorbent from outside the tube wall using an external magnet after the completion of the adsorption process.

■ RESULTS AND DISCUSSION

FTIR Analysis

FTIR spectra of uncoated magnetite, magnetite-CTAB-0.01, magnetite-CTAB-0.05, and magnetite-CTAB-0.10 (Fig. 1) show the peak at wavenumbers of 572, 586, 586, and 590 cm^{-1}, which is characteristic for the stretching vibration of the Fe–O bond on magnetite [21-22]. The shift of Fe-O absorption from 572 cm^{-1} in uncoated magnetite to 586–590 cm^{-1} in magnetite-CTAB indicates the alterations in the surface environment of MNPs caused by an interaction between the MNPs and the adsorbed CTAB molecules [3]. The weak adsorption at 3400 cm^{-1} in all spectra was caused by stretching vibration of $O–H^-$ adsorbed on the MNPs surface, while the peak at 1627 cm^{-1} comes from the bending vibration of the hydroxyl group on the adsorbed water [22].

In Fig. 1(b-d), the peaks appearing at wavenumbers of 2924 and 2854 cm^{-1} are due to the –CH and $–CH_3$ vibrations from CTAB, respectively [7,22]. Also, the bending vibration bands of the head $[N(CH_3)_3]$ group at 1481 cm^{-1} and (CN^+) stretching vibrations at 904 cm^{-1} are observed [23]. The intensity of peaks increases with the increase in the CTAB mass added. As the concentration of CTAB used in this synthesis was relatively small, the absorptions associated with CTAB in Fig. 1(b) are relatively weak, indicating that only a few portions of CTAB coat the magnetite particles.

XRD Analysis

The diffractograms of uncoated magnetite, magnetite-CTAB-0.01, magnetite-CTAB-0.05, and magnetite-CTAB-0.10 (Fig. 2) show multiple peaks at 2θ

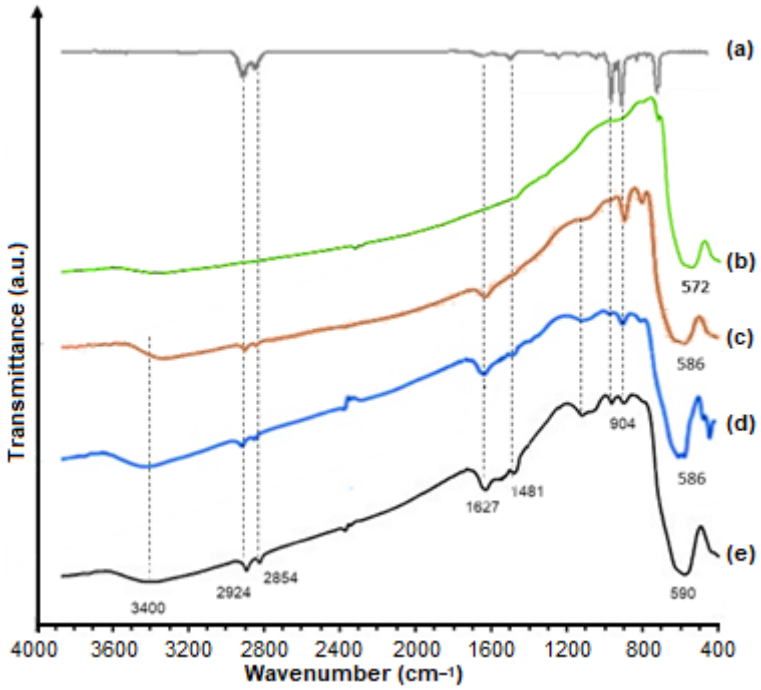

Fig 1. FTIR spectra of (a) CTAB, (b) uncoated magnetite, (c) magnetite-CTAB-0.01, (c) magnetite-CTAB-0.05, (d) magnetite-CTAB-0.10

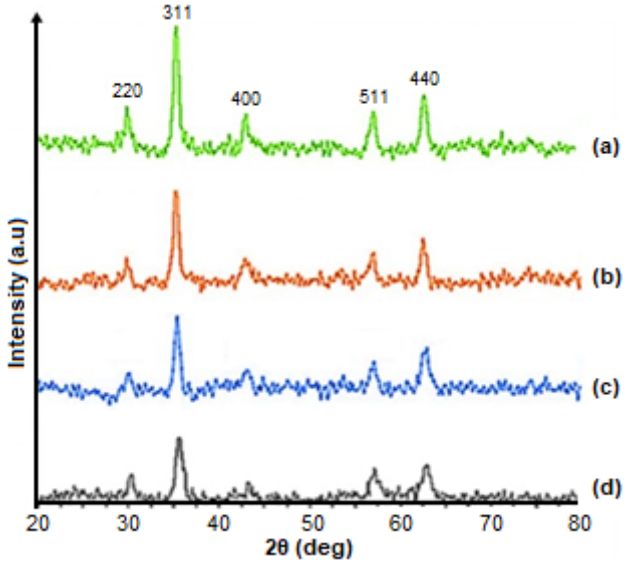

Fig 2. Diffractograms of (a) uncoated magnetite, (b) magnetite-CTAB-0.01, (c) magnetite-CTAB-0.05, and (d) magnetite-CTAB-0.10

30.5, 35.62, 43.07, 57.18, and 62.75° which correspond to *d*-spacing of 2.93, 2.52, 2.9, 1.61, and 1.48 Å, respectively. These peaks are the characteristics of the inverted spinel phase of magnetite, namely (220), (311), (400), (511), and (440) of magnetite (ICDD No.85-1436) [24], indicating clearly that the four samples contain magnetite material. The identical diffraction angles among the diffractograms show that the CTAB coating does not affect the magnetite crystal structure. Hence, the CTA^+ cation interacts electrostatically only with the surface charge of the MNPs and does not form covalent bonds with atoms in the magnetite crystal system. The decrease in peak intensity after the coating is caused by fewer X-rays reaching the MNP surface.

In the magnetite-CTAB-0.01 sample (Fig. 2(b)), the peak is still relatively high, indicating that only a few portions of the MNP were coated by CTAB, which matches the interpretation of FTIR spectra. In the magnetite-CTAB-0.05 sample (Fig. 2(c)), the diffractogram peaks were still observed, albeit at a lower intensity, indicating that the inverted spinel of magnetite is still present in the sample. Meanwhile, the intensity decreases significantly in the 0.10 magnetite-CTAB sample (Fig. 2(d)), indicating that the CTAB coating has been perfectly obtained. Based on the Scherrer Equation [25], namely $D = K\lambda/(\beta\cos\theta)$ where K is the constant (0.94), λ is the wavelength of X-ray (0.15418 nm), β is the FWHM of the (311) peak, and θ is the diffraction angle,

it is observed the average crystal sizes of magnetite decrease in the order of uncoated magnetite, magnetite-CTAB-0.01, magnetite-CTAB-0.05, and magnetite-CTAB-0.10, e.g., about 43, 35, 28, and 23 nm, respectively. This decrease in crystallite size with the increasing addition of CTAB is due to the role of CTAB in blocking the agglomeration among MNPs. Therefore, it is easily understood that increasing the addition of CTAB results in a smaller crystallite size of MNPs because the formation of agglomerates is hindered by CTAB.

VSM Analysis

VSM analysis was conducted only for the sample showing the best performance in the preliminary test (magnetite-CTAB-0.10) and uncoated magnetite for comparison. The hysteresis curves of uncoated magnetite and magnetite-CTAB-0.10 presented in Fig. 3 show that the saturation magnetization field (Ms) of the two samples are 72.8 and 49.2 emu g^{-1}, respectively. The Ms value of magnetite-CTAB-0.10 is smaller than that of uncoated magnetite due to the presence of non-magnetic coating materials, i.e., CTAB, that reduces the magnetic properties [26]. This VSM result is in line with the results of the diffractogram observations, showing the peak intensity of magnetite-CTAB-0.10 diffractogram is lower than that of uncoated magnetite. The magnetite-CTAB-0.10 composite has superparamagnetic properties, as indicated by the absence of loops in its hysteresis curve (Fig. 3(b)) [27]. Superparamagnetic materials arise from very small ferromagnetic materials (< 25 nm) that form magnetic domains with high degrees of freedom. This result matches the estimated crystallite size of MNPs based on the previously stated Scherer Equation (23 nm). The uncoated magnetite in this study is ferrimagnetic, as indicated by the presence of loops on its hysteresis curve (Fig. 3(a)) [28]. This fact is due to the agglomeration of the existing MNPs so that the particle size becomes relatively large. Agglomeration between MNPs in magnetite-CTAB-0.10 composite does not occur because the CTAB layer blocks the formation of agglomerates.

SEM Analysis

Similar to VSM analysis, SEM analysis was also carried out to magnetite-CTAB-0.10 and uncoated magnetite. The SEM image of uncoated magnetite (Fig. 4(a)) shows the presence of lumps of relatively large size in around 8–16 μm with an average of 9.94 ± 0.38 μm, resembling peeling bark and cast stone fragments. Meanwhile, the image of magnetite-CTAB-0.10 (Fig. 4(b)) shows relatively small grains (2–13 μm with an average of 6.56 ± 0.45 μm) and resembling a pile of gravel mixed with sand. In uncoated magnetite, the magnetite particles are agglomerated because of their magnetic properties. In the magnetite-CTAB-0.10, however, XRD diffractogram data are corroborated by VSM data, confirming that the crystallite size of magnetite in the core of the particle was about 23 nm. On the other hand, the SEM image shows that the particle size of Magnetite-CTAB-0.10 is about 2–10 μm or 2,000–10,000 nm. Based on this finding, it is argued that what looks like a tiny grain in Fig. 4(b) is not just a magnetite-CTAB micelle but possibly an agglomeration of hundreds to thousands of magnetite-CTAB micelles.

Preliminary Determination of Adsorption Capacity

The adsorption capacity of MO and MV on uncoated magnetite, magnetite-CTAB-0.01, magnetite-CTAB-0.05, and magnetite-CTAB-0.10 are presented in

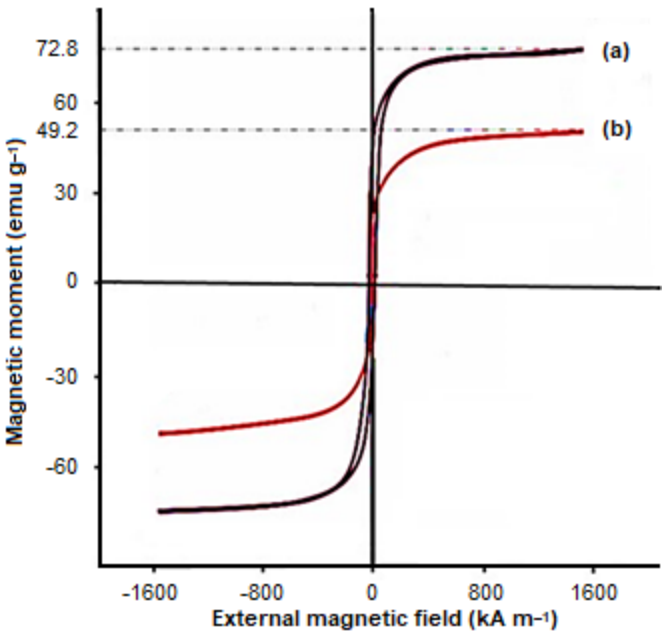

Fig 3. Magnetization curve of (a) uncoated magnetite and (b) magnetite-CTAB-0.10

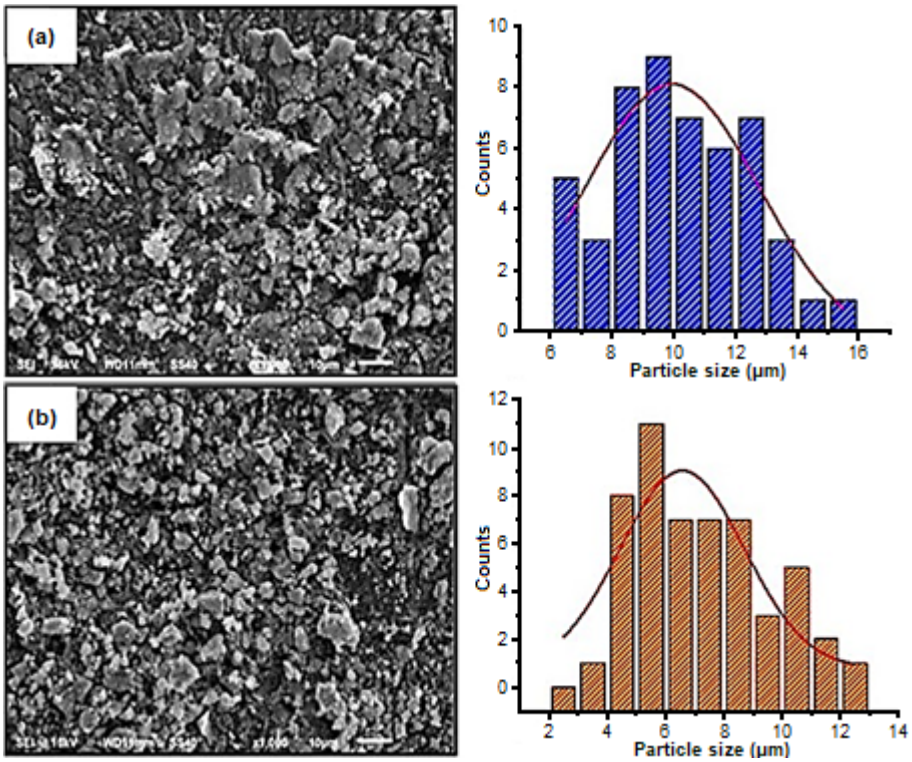

Fig 4. SEM images and the particle size distribution processed by ImageJ software: (a) uncoated magnetite and (b) magnetite-CTAB-0.10

Table 1. These data are needed to determine the optimum CTAB concentration in the synthesis of magnetite-CTAB composites. The magnetite-CTAB with a certain CTAB concentration with the highest adsorption capacity is considered the optimum CTAB addition concentration. The adsorption of the cationic dye of MV in this experiment was intended to check the selectivity of the adsorbents towards cationic and anionic dyes. From Table 1, it is found that increasing the concentration of CTAB in the synthesis of magnetite-CTAB gives rise to the increase in adsorption capacity. Based on these adsorption capacity data, the structure of magnetite-CTAB may be estimated. The uncoated magnetite provides a relatively small adsorption capacity because at the condition of adsorption, pH = 7 (a little bit higher than PZC), its surface has a negative charge so that it repels each other with an anionic dye of MO, while cationic dye of MV is sufficiently adsorbed because it has opposite charge with the surface of adsorbents.

Along with the increase in the concentration of CTAB, adsorption of anionic MO increases significantly

Table 1. Adsorption capacity (mg g^{-1}) and efficiency (%) of MO and MV on uncoated magnetite, magnetite-CTAB-0.01, magnetite-CTAB-0.05, and magnetite-CTAB-0.10

Adsorbent	Adsorption capacity, mg g^{-1} (% efficiency)	
	MO	MV
Uncoated magnetite	0.41 (5.20)	2.31 (28.9)
Magnetite-CTAB-0.01	5.48 (68.6)	0.50 (6.30)
Magnetite-CTAB-0.05	7.81 (97.6)	0.43 (5.38)
Magnetite-CTAB-0.10	7.94 (99.2)	0.14 (1.76)

while that of cationic MV sharply decreases. This is because the surface charge of the adsorbents changes gradually from negatively charged to positively charged surfaces as the double layer of CTAB is formed on the surface. The lower adsorption capacity of magnetite-CTAB-0.01 towards MO (5.48 mg g^{-1} or 68.55%) compared to the other two magnetite-CTAB adsorbents (almost 100% MO is adsorbed) indicates that the number of MNPs coated by CTAB is relatively still low or in other words, the concentration of CTAB in the

reaction system is still not enough to form a perfect double layer. This is consistent with the FTIR analysis that shows the absorption spectra of the CTA^+ group to be relatively weak. Also, the high intensity of the XRD diffractogram indicates that only a few MNPs are coated by CTAB. On the other hand, the adsorption capacity of magnetite-CTAB-0.05 and magnetite-CTAB-0.10 is 7.81 mg g^{-1} (97.6%) and 7.94 mg g^{-1} (99.2%), respectively, meaning that all MO is adsorbed from the solution and that the double-layer micelles were fully formed.

The magnetite-CTAB has a positive charge of $(CH_3)_3N^+$ group at the surface of adsorbents. This favorably interacts with anionic dyes of MO through electrostatic interaction [10]. The positive polar is formed on the surface of the Magnetite-CTAB composite because the CTA^+ ions form double-layered spherical micelles with MNPs located in the core. In the first layer, the polar group of $(CH_3)_3N^+$ from CTA^+ interact electrostatically with the negative charge on the surface of MNPs, while the alkyl chain as the nonpolar group interacts hydrophobically with the alkyl chain of CTA^+ in the second layer. The positive polar groups of the second layer point to the micelle surface to interact electrostatically with the anionic die of MO [23]. Fig. 5 presents the hypothetical structure of the double layer micelles on Magnetite-CTAB and the interactions that emerge between the positively charged surface of the adsorbent and the anionic adsorbate.

Table 1 clearly shows that the adsorption capacity of all adsorbents towards cationic MV is relatively low compared to the adsorption percentage of MO except uncoated magnetite. The relatively large adsorption capacity (2.31 mg g^{-1} or 28.9%) of uncoated magnetite towards MV is due to electrostatic interaction between the negative charge of the uncoated magnetite surface with the positive charge of the MV. However, this adsorption capacity value is still much lower than the adsorption capacity of Magnetite-CTAB-0.10 towards MO (7.94 mg g^{-1} or 99.21%). This is probably caused by steric hindrance between MV molecules due to the relatively small size of uncoated MNPs. In the case of magnetite-CTAB adsorbents, the greater the concentration of CTAB used in the magnetite-CTAB synthesis, the smaller its adsorption capacity towards cationic MV. It is because more positive charges are formed on the magnetite surface so that a stronger repulsion occurs between cationic MV and the surface of the adsorbent. MV dye in these conditions of experiment produces cationic dye. Therefore, the most suitable adsorbent to adsorb MV is an anionic adsorbent. This finding also indirectly confirms that the developed adsorbent of magnetite-CTAB is charge-selective adsorbent or cationic adsorbent. For this reason, further study of MO adsorption was conducted only on magnetite-CTAB-0.10.

Solution pH is an essential factor in the adsorption

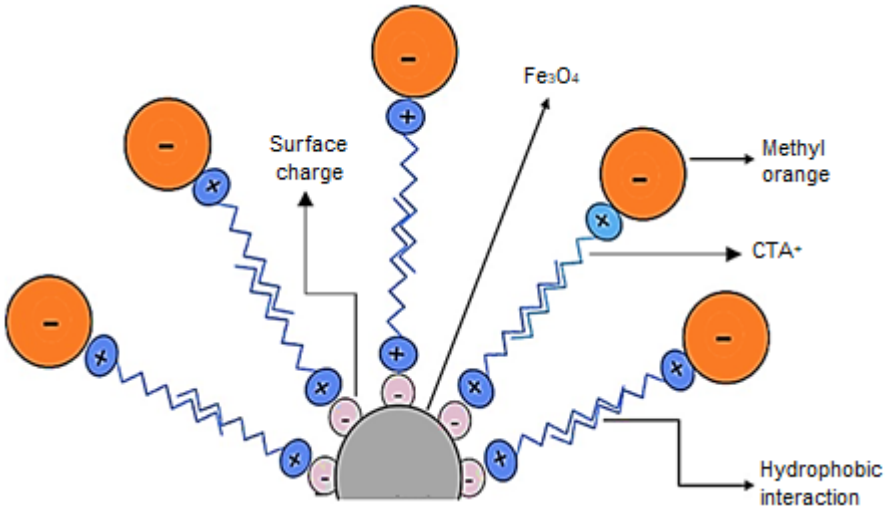

Fig 5. Hypothetical structure of double layer micelles on Magnetite-CTAB and its interaction with MO

process because it affects the surface charge of magnetite-CTAB composites and MO speciation [16]. Fig. 6 shows that the adsorption capacity increases with increasing pH of the solution from 4 to 7, then it continues to decrease from 7 to 9. The optimum adsorption occurs at pH 7 with an adsorption capacity of 7.27 mg g^{-1} (90.82%). Under acidic conditions, the MO molecule is protonated to form a quinoid structure with a positive charge on its NH_2 group (Fig. 7), while the surface of the adsorbent is also positively charged. Therefore, at low pH, repulsion between the protonated MO molecules and the positive charge of magnetite-CTAB-0.10 occurs, leading to lower adsorption of MO by magnetite-CTAB-0.10 with the decrease in solution pH from 7 to 4. Fig. 6 also shows that the adsorption capacity decreases significantly with increasing pH from 7 to 9. This is due to competition between the negatively charged MO molecules and OH^- ions to electrostatically interact with a positive charge at magnetite-CTAB-0.10 under alkaline conditions.

Adsorption Kinetics

The effect of contact time on the adsorption capacity of MO by magnetite-CTAB-0.10 is presented in Fig. 8. It is clearly shown the adsorption takes place very rapidly at the beginning. There are still plenty of active sites on the adsorbent that can interact with the MO, and the MO concentration in the solution is still high. The adsorption reaches its equilibrium after 120 min of mixing, where the amount of adsorbed MO no longer increases, meaning that the adsorption capacity (q_t) has reached its maximum value. There are two possible factors: saturation of the active sites or the exhaustion of adsorbent. As the concentration and volume of MO solution used in this study are relatively low (20 mL of 10 mg L^{-1}), the second factor is more likely in this case.

Adsorption kinetics is used to predict the adsorption rate constant (k), providing important information about the mechanism and model of the adsorption process. In this study, three well-known adsorption kinetic models were applied to evaluate the most appropriate kinetic models: pseudo-first-order (Lagergren), pseudo-second-order (Ho and McKay), and Langmuir-Hinshelwood. The linear form of Lagergren's adsorption kinetics model is presented in Eq. (2) [30]:

$$\ln(q_e - q_t) = \ln q_e - k_1 t \quad (2)$$

where k_1 (min^{-1}) is the apparent first-order rate constant, q_e (mol g^{-1}) is the number of moles of adsorbate adsorbed by each gram of adsorbent at equilibrium, and q_t (mol g^{-1}) is the number of moles of adsorbate adsorbed by per gram of adsorbent at time t. If the plot of ln (q_e – q_t) versus t is constructed and the data fit the model, then a linear curve will be obtained with ln q_e as the intercept

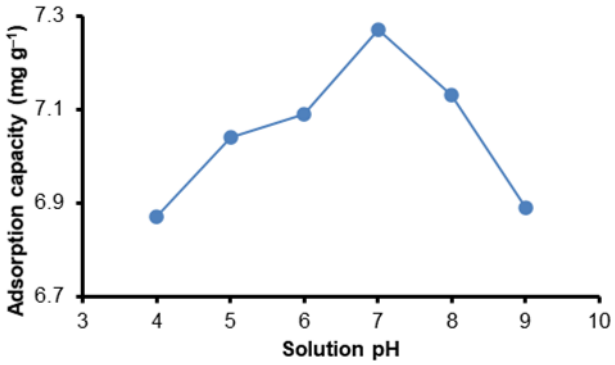

Fig 6. Effect of solution pH on the adsorption capacity of MO on magnetite-CTAB-0.10

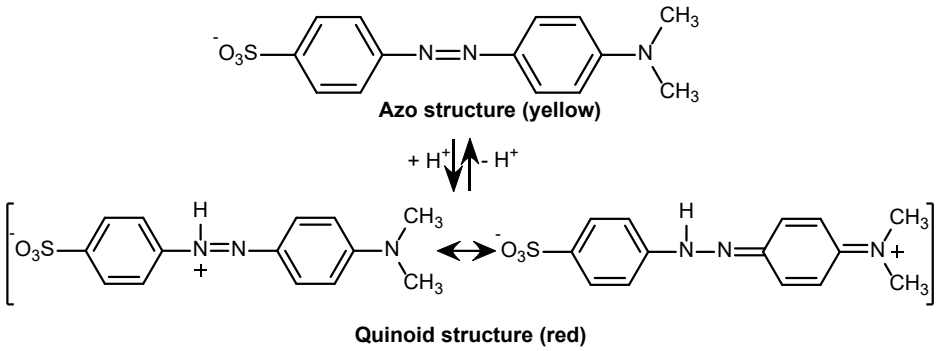

Fig 7. The resonance structure of MO as a function of pH [29]

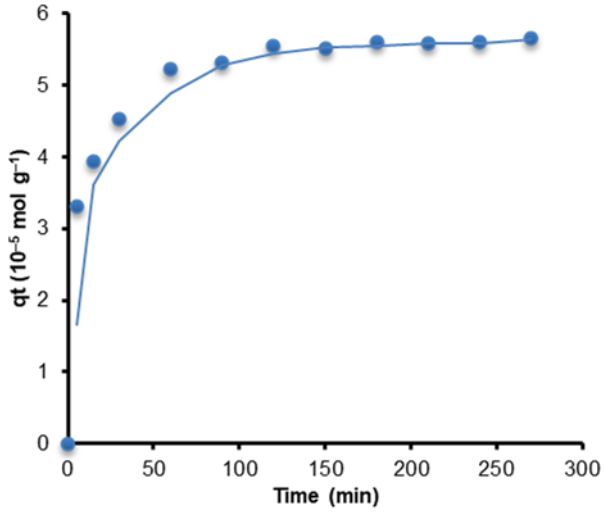

Fig 8. The effect of contact time on the adsorption capacity of MO

and k_1 as the slope.

The linear form of Ho and McKay's adsorption kinetics model is represented by Eq. (3) [31].

$$\frac{t}{q_t} = \frac{1}{k_2 q_e^2} + \frac{t}{q_e} \quad (3)$$

where k_2 is the adsorption rate constant of Ho and McKay (g mol^{-1} min), q_e is the amount of MO adsorbed at equilibrium (mol g^{-1}), and q_t is the amount of MO adsorbed at time t (mol g^{-1}). If t/q_t was plotted as a function of t and the data fit the model, then a linear curve will be obtained with $1/q_e$ as the intercept and $\frac{1}{k_2 q_e^2}$ as the slope so that the values of q_e and k_2 can be calculated.

Meanwhile, the linear form of the Langmuir-Hinshelwood adsorption kinetics model is expressed in Eq. (4) [32].

$$\frac{\ln\left(\frac{C_o}{C_t}\right)}{C_o - C_t} = k1\frac{t}{C_o - C_t} - k_o \quad (4)$$

where C_o (mol L^{-1}) is the initial concentration of adsorbate, C_t (mol L^{-1}) is the concentration of adsorbate remaining after adsorption for t time, k_1 (min^{-1}) is the adsorption rate constant, and k_o (L mol^{-1}) is the adsorption equilibrium constant. If a curve of $[\ln (C_o/C_t)]/(C_o-C_t)$ versus $t/(C_o-C_t)$ is constructed, then a linear curve with k_1 as the slope and $-k_o$ as the intercept will be obtained if the adsorption follows the kinetic adsorption model. Detailed results of the evaluation of the kinetic model by the three equations are presented in Table 2.

From Table 2, it is easily seen that Ho and McKay's kinetic model gives the highest value of correlation coefficient (r^2), 0.9995, compared to those produced by the other two kinetic models, indicating that the MO adsorption on magnetite-CTAB-0.10 is best fitted to the Ho and McKay kinetic model. This suggests that at least two factors are involved in the mechanism of MO adsorption on the adsorbents, possibly the adsorbate and the active sites of the adsorbent and/or molecule of the solvent. Applying this model, it is found that the amount of MO adsorbed at equilibrium (q_e) is 5.73×10^{-5} mol g^{-1}, and the adsorption rate constant (k_2) is 3.54×10^3 g mol^{-1} min. The linear curve of t/q_t versus t is attached as the Supporting Information (Fig. S1).

Adsorption Isotherms

The curve for the amount of MO adsorbed at equilibrium (q_e) as a function of initial concentration [MO] is given in Fig. 9. It is observed that the q_e value increases with the increasing initial [MO], then it reaches the saturation state at [MO] of 35 mg/L, giving a maximum adsorption capacity of 26.33 mg g^{-1}. The MO adsorption isotherm on magnetite-CTAB-0.10 was studied using two types of well-known isotherm equation models, i.e., the Langmuir and Freundlich adsorption isotherm models.

The linear form of the Langmuir Isotherms equation is presented in Eq. (5) [33], where C_e (mol L^{-1}) is the concentration of adsorbate in the solution at

Table 2. Parameters of three kinetic models in MO adsorption on magnetite-CTAB-0.10

Kinetic models	Parameters	Values
Pseudo first order (Lagergren)	r^2	0.9639
	q_e (mol g^{-1})	2.389×10^{-5}
	k_1 (min^{-1})	2.83×10^{-2}
Pseudo second order (Ho and McKay)	r^2	0.9995
	q_e (mol g^{-1})	5.73×10^{-5}
	k_2 (g mol^{-1} min)	3.54×10^3
Langmuir-Hinshelwood	r^2	0.6159
	k_1 (min^{-1})	6×10^{-3}

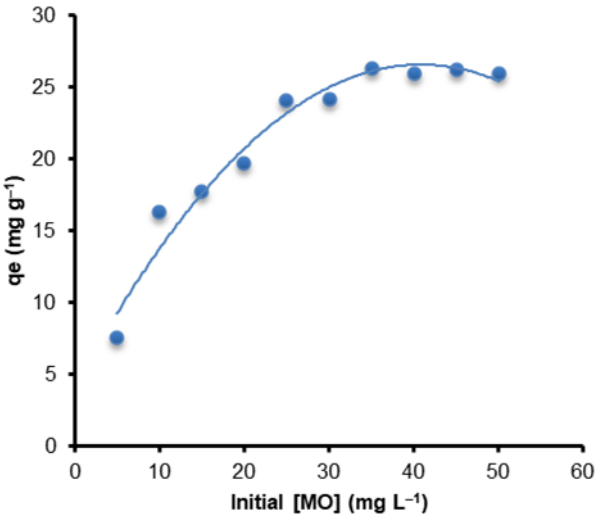

Fig 9. The curve of q_e as a function of the initial [MO]

equilibrium, q_e (mol g^{-1}) is the mole of adsorbate adsorbed by each gram of adsorbent at equilibrium, q_m (mol g^{-1}) is the maximum adsorption capacity, and K_L (L mol^{-1}) is the Langmuir constant. Based on Eq. (5), the plot of C_e/q_e vs. C_e will be linear with $1/q_m$ as the slope and $1/(q_m K_L)$ as the intercept if the adsorption follows this model so that the values of K_L and q_m can be obtained. An approximation of adsorption energy can be determined based on the standard Gibbs equation of $\Delta G_{ads}^0 = -RT \ln K_L$, where ΔG_{ads}^0 is the standard Gibbs free energy of adsorption, R is the universal gas constant (8.314 J K^{-1} mol^{-1}), and T is the temperature in Kelvin.

$$\frac{C_e}{q_e} = \frac{1}{q_m K_L} + \frac{1}{q_m} C_e \quad (5)$$

Meanwhile, the linear equation for Freundlich adsorption isotherms is expressed in Eq. (6) [34], where C_e is the concentration of adsorbate at equilibrium (mol L^{-1}), q_e is the amount of adsorbed substance in a gram of adsorbent (mol g^{-1}), K_F is the Freundlich adsorption capacity (mol g^{-1}) and n is a constant.

$$q_e = \log K_F + \frac{1}{n} \log C_e \quad (6)$$

The linear curves of the Langmuir and Freundlich Isotherms are attached in Fig. S2 and Fig. S3), respectively. Table 3 gives detailed isotherm parameter calculations for the two models used in this study. Because the value of r^2 for the Langmuir Isotherms (0.9926) is greater than that for the Freundlich Isotherms (0.8252), it can be concluded that the Langmuir Isotherm model best describes the adsorption of MO on Magnetite-CTAB-0.10. These results suggest that the adsorption occurs on more homogeneous surfaces, probably due to the double-layer formation of CTAB, namely the polar group of CTA^+ on the core-shell of magnetite-CTAB. In addition, according to Fig. 9, the maximum adsorption is reached at a concentration of 35 mg L^{-1}, and, afterward, the adsorption tends to be constant. This indicates that the surface of the adsorbent experiences saturation when all of the active sites have been filled with MO, and the adsorption process will no longer occur even when the concentration of MO increases because adsorption is limited to one layer only.

Table 3 shows that the maximum adsorption capacity (q_{max}) of MO is 27.9 mg g^{-1}, meaning that every 1 g of the adsorbent can adsorb 27.9 mg of MO. This q_{max} value of MO is higher than those reported by previous studies that used various adsorbents. Table 4 gives the q_{max} of MO using the present adsorbent of Magnetite-CTAB-0.10 along with those obtained by other workers [17-19, 35-37] for comparison. It is clearly found that the adsorbent developed in this study, magnetite-CTAB-0.10, is superior and more efficient compared to previously reported adsorbents as it gives the highest value of q_{max}. Even more, it is almost four times higher than that of previously reported magnetite-CTAB [19], which was synthesized using the conventional method without optimization of the concentration of CTAB, without keeping the inert atmosphere, and using conventional magnetic mixing. The value of adsorption capacity obtained from this study is also compared to the results obtained from many studies using different magnetite absorbents, as summarized in Table 5. It is

Table 3. Adsorption isotherm parameters of MO on Magnetite-CTAB-0.10

Isotherms model	Parameter	Value
Langmuir	r^2	0.9926
	q_{max} (mg g^{-1})	27.9
	K_L (L mol)	7.46×10^4
	ΔG_{ads}^0 (kJ mol^{-1})	−27.8
Freundlich	r^2	0.8252
	n	3.90
	K_F (L g^{-1})	8.91×10^{-4}

Table 4. Comparison of maximum adsorption capacities (q_{max}) for MO on various types of adsorbents

Adsorbents	q_{max} (mg g^{-1})	References
Copper oxide	1.2	[35]
Ammonium-functionalized MCM-41	1.12	[36]
Wheat Bran	12	[17]
Cork powder	16.8	[18]
Activated aluminas	9.8	[37]
Magnetite-CTAB	7.58	[19]
Magnetite-CTAB (modified method)*	27.9	This study

*CTAB concentration is optimized, synthesized in an inert atmosphere, and used ultrasonic mixing to speed up synthesis

Table 5. Comparison of maximum adsorption capacities (q_{max}) for MO on various types of magnetite adsorbents

Adsorbent types	Optimum pH	Equilibrium time (min)	Q_{max} (mg g^{-1})	Magnetization (emu g^{-1})	References
Magnetic hydroxyapatite	7	80	18.0	12.5	[38]
γ-Fe_2O_3/2C nanocomposite	4.5	60	42.34	30	[39]
Magnetic cellulose beads	7	180	1.47	40	[40]
Magnetic halloysite nanotubes/iron oxide composites	7	480	0.65	27.91	[41]
Rectorite/iron oxide nanocomposites	7	1	0.36	19.14	[42]
γ-Fe_2O_3 crosslinked chitosan composite	6.6	100	29.46	4.36	[43]
Magnetite-CTAB	7	120	27.9	49.2	This study

observed that our results, in general, are higher or comparable to those previously reported in many kinds of literature [38-43].

Moreover, based on the equation of $\Delta G_{ads}^0 = -RT \ln K_L$ [44], where the values of R = 8.314 J K^{-1} mol^{-1}, T = 298.15 K, and $K_L = 7.46 \times 10^4$ L mol^{-1}, it has been found that the value of ΔG_{ads}^0 is −27.8 kJ mol^{-1}. This result indicates that the adsorption of MO on Magnetite-CTAB-0.10 is dominated by both physisorption and chemisorption mechanisms (ΔG_{ads}^0 ranges from −20 to −80 kJ mol^{-1} [45-46]). It is predicted that the primary interaction in this adsorption is an electrostatic interaction between the positive surface charge on the adsorbent and the negative charge group on the adsorbate. Besides that, the relatively weak Van der Waals force may also be expected.

Recovery Test

The visualization (photograph) of the experimental bottle used in the recovery test after the separation process of the used adsorbent with an external magnetic field is given in the Supporting Information (4). The adsorbent separation lasted only 1 min. The adsorbent magnetite-CTAB-0.10 and the adsorbed MO were attracted strongly by an external magnetic field and stuck to the bottle wall. This case matches the results of VSM measurements, which show that the magnetite-CTAB-0.10 composite is superparamagnetic with a large M_s of 68.88 emu g^{-1}. The orange solution containing MO becomes clear quickly because the composite rapidly adsorbs MO with a k_2 of 3.54×10^3 g mol^{-1} min and a K_L of 7.46×10^4 L mol. Furthermore, the adsorbent used and the adsorbed MO can be separated immediately by the external magnetic field.

■ CONCLUSION

Rapid synthesis of Magnetite-CTAB composites has been successfully developed by the coprecipitation method using ultrasonic mixing in an inert atmosphere. The use of 0.10 M CTAB produces the best performance of the magnetite-CTAB composite for the adsorption of methyl orange, probably due to the formation of a

double layer spherical micellar structure with MNPs as the core and a double layer of CTAB as the shell. The magnetite-CTAB composite obtained has a strong superparamagnetic property with a saturation magnetization field (Ms) of 49.2 emu g^{-1}. Adsorption study of MO using the developed adsorbent suggests the material can adsorb anionic dye of MO efficiently with the optimum conditions reached at pH 7 and 120 min of contact time. Kinetic study of the adsorption indicates that adsorption of MO on magnetite-CTAB fits well into the pseudo 2nd order kinetic model, meaning at least two factors are involved in the mechanism of adsorption, possibly the adsorbate itself and the active site and/or the molecules of solvent. The adsorption isotherms of MO by Magnetite-CTAB composite are best described by the Langmuir isotherm model, suggesting that the adsorption takes place on the homogenous active sites of the adsorbent surface and forms a monolayer. As the adsorbent selectively adsorbed anionic dyes (MO) over cationic ones (MV), it is predicted that the active sites are the positively charged group of CTA^+ in the second layer facing outside the micellar. The developed Magnetite-CTAB composite is very prospective and promising because it selectively adsorbs anionic species and can be easily and quickly separated from the solution using an external magnetic field after the adsorption process. Therefore, it may be applied not only to anionic dyes but also to other hazardous anionic species in the environment.

■ ACKNOWLEDGMENTS

The first author (Nor Harisah) would like to acknowledge the Bureau of planning and overseas cooperation, The Ministry of Education and Culture of the Republic of Indonesia, for the financial support through "Beasiswa Unggulan" for M.Sc. Program in Chemistry at Universitas Gadjah Mada under the cooperation agreement letter No. 53960/A1.4/LL/2016 dated 30 September 2016.

■ REFERENCES

[1] Mahdavi, M, Ahmad, M.B., Haron, M.J., Namvar, F., Nadi, B., Ab Rahman, M.Z., and Amin, J., 2013, Synthesis, surface modification and characterisation of biocompatible magnetic iron oxide nanoparticles for biomedical applications, *Molecules*, 18 (7), 7533–7548.

[2] Gan, L., Lu, Z., Cao, D., and Chen, Z., 2018, Effects of cetyltrimethylammonium bromide on the morphology of green synthesized MNPsused to remove phosphate, *Mater. Sci. Eng., C*, 82, 41–45.

[3] Khoshnevisan, K., Barkhi, M., Zare, D., Davoodi, D., and Tabatabaei, M., 2012, Preparation and characterization of CTAB-coated Fe_3O_4 nanoparticles, *Synth. React. Inorg., Met.-Org., Nano-Met. Chem.*, 42 (5), 644–648.

[4] Lellis, B., Fávaro-Polonio, C.Z., Pamphile, J.A., and Polonio, J.C., 2019, Effects of textile dyes on health and the environment and bioremediation potential of living organisms, *Biotechnol. Res. Innovation*, 3 (2), 275–290.

[5] Rajabi, A.A., Yamini, Y., Faraji, M., and Nourmohammadian, F., 2016, Modified magnetite nanoparticles with cetyltrimethylammonium bromide as superior adsorbent for rapid removal of the disperse dyes from wastewater of textile companies, *Nanochem. Res.*, 1 (1), 49–56.

[6] Aquino, J.M., Rocha-Filho, R.C., Ruotolo, L.A.M., Bocchi, N., and Biaggio, S.R., 2014, Electrochemical degradation of a real textile wastewater using β-PbO_2 and DSA® anodes, *Chem. Eng. J.*, 251, 138–145.

[7] Khatri, J., Nidheesh, P.V., Anantha Singh, T.S., and Kumar, M.S., 2018, Advanced oxidation processes based on zero-valent aluminium for treating textile wastewater, *Chem. Eng. J.*, 348, 67–73.

[8] Sabna, V., Thampi, S.G., and Chandrakaran, S., 2018, Adsorptive removal of cationic and anionic dyes using graphene oxide, *Water Sci. Technol.*, 78 (4), 732–742.

[9] Kasperchik, V.P., Yaskevich, A.L., and Bil'dyukevich, A.V., 2012, Wastewater treatment for removal of dyes by coagulation and membrane processes, *Pet. Chem.*, 52 (7), 545–556.

[10] Estelrich, J., Escribano, E., Queralt, J., and Busquets, M.A., 2015, Iron oxide nanoparticles for

magnetically-guided and magnetically-responsive drug delivery, *Int. J. Mol. Sci*., 16 (4), 8070–8101.

[11] Zemtsova, E.G., Ponomareva, A.N., Panchuk, V.V., Galiullina, L.F., and Smirnov, V.M., 2017, Synthesis, structure and magnetic properties of magnetite-SiO_2 nanocomposites with core-shell structures for targeted drug delivery, *Rev. Adv. Mater. Sci*., 52, 82–90.

[12] Kristianto, H., Reynaldi, E., Prasetyo, S., and Sugih, A.K., 2020, Adsorbed leucaena protein on citrate modified magnetite nanoparticles: Synthesis, characterization, and its application as magnetic coagulant, *Sustainable Environ. Res.*, 30 (1), 32.

[13] Yew, Y.P., Shameli, K., Miyake, M., Kuwano, N., Bt Ahmad Khairudin, N.B., Bt Mohamad, S.E., and Lee, K.X., 2016, Green synthesis of magnetite (Fe_3O_4) nanoparticles using seaweed (*Kappaphycus alvarezii*) extract, *Nanoscale Res. Lett.*, 11 (1), 276.

[14] El-Dib, F.I., Mohamed, D.E., El-Shamy, O.A.A., and Mishrif, M.R., 2020, Study the adsorption properties of magnetite nanoparticles in the presence of different synthesized surfactants for heavy metal ions removal, *Egypt. J. Pet.*, 29 (1), 1–7.

[15] Huang, R., Liu, Q., Huo, J., and Yang, B., 2017, Adsorption of methyl orange onto protonated cross-linked chitosan, *Arabian J. Chem.*, 10, 24–32.

[16] Subasioglu, T., and Bilkay, I.S., 2009, Determination of biosorption conditions of methyl orange by humicolafuscoatra, *J. Sci. Ind. Res.*, 68, 1075–1077.

[17] Alzaydien, A.S., 2015, Adsorption behavior of methyl orange onto wheat bran: Role of surface and pH, *Orient. J. Chem*., 31 (2), 643–651.

[18] Krika, F., and Benlahbib, O.F., 2015, Removal of methyl orange from aqueous solution via adsorption on cork as a natural and low-cost adsorbent: Equilibrium, kinetic and thermodynamic study of the removal process, *Desalin. Water Treat.*, 53 (13), 3711–3723.

[19] Fisli, A., Winatapura, D.S., and Alfian, A., 2018, The surface functionalization of Fe_3O_4 nanoparticles by CTAB as adsorbent for methyl orange elimination in water, *J. Phys.: Conf. Ser.*, 1091, 012002.

[20] Edet, U.A., and Ifelebuegu, A.O., 2020, Kinetics, isotherms, and thermodynamic modeling of the adsorption of phosphates from model wastewater using recycled brick waste, *Processes*, 8 (6), 665.

[21] Gaffer, A., Al Kahlawy, A.A., and Aman, D., 2017, Magnetic zeolite-natural polymer composite for adsorption of chromium (VI), *Egypt. J. Pet.*, 26 (4), 995–999.

[22] Guivar, J.A.R., Sanches, E.A., Magon, C.J., and Fernandes, E.G.R., 2015, Preparation and characterization of cetyltrimethylammonium bromide (CTAB)-stabilized Fe_3O_4 nanoparticles for electrochemistry detection of citric acid, *J. Electroanal. Chem.*, 755, 158–166.

[23] Elfeky, S.A., Mahmoud, S.E., and Youssef, A.F., 2017, Applications of CTAB modified magnetic nanoparticles for removal of chromium (VI) from contaminated water, *J. Adv. Res*., 8 (4), 435–443.

[24] Viana, R.B., da Silva, A.B.F., and Pimentel, A.S., 2012, Infrared spectroscopy of anionic, cationic, and zwitterionic surfactants, *Adv. Phys. Chem*., 2012, 903272.

[25] Muniz, F.T., Miranda, M.A.R., Dos Santos, C.M., and Sasaki, J.M., 2016, The Scherrer equation and the dynamical theory of X-ray diffraction, *Acta Crystallogr., Sect. A: Found. Adv.*, 72 (3), 385–390.

[26] Liu, Y., 2013, Recent progress in Fourier transform infrared (FTIR) spectroscopy study of compositional, structural and physical attributes of developmental cotton fibers, *Materials*, 6 (1), 299–313.

[27] Faghihian, H., Moayed, M., Firooz, A., and Iravani, M., 2014, Evaluation of a new magnetic zeolite composite for removal of Cs^+ and Sr^{2+} from aqueous solutions: Kinetic, equilibrium and thermodynamic studies, *C.R. Chim.*, 17 (2), 108–117.

[28] Baumgartner, J., Bertinetti, L., Widdrat, M., Hirt, A.M., and Faivre, D., 2013, Formation of MNPsat low temperature: from superparamagnetic to stable single-domain particles, *PLoS One*, 8 (3), e57070.

[29] Kahlert, H., Meyer, G. and Albrecht, A., 2016, Colour maps of acid-base titrations with colour indicators: how to choose the appropriate indicator and how to estimate the systematic titration errors, *ChemTexts*, 2 (2), 7.

[30] Kajjumba, G.W., Emik, S., Öngen, A., Özcan, H.K., Aydın, S., 2018, "Modelling of Adsorption Kinetic Processes–Errors, Theory, and Application" in *Advanced Sorption Process Applications*, Eds. Edebali, S., IntechOpen, Rijeka, Croatia.

[31] Aliakbarian, B., Casazza, A.A., and Perego, P., 2015, Kinetic and isotherm modelling of the adsorption of phenolic compounds from olive mill wastewater onto activated carbon, *Food Technol. Biotechnol.*, 53 (2), 207–214.

[32] Armenise, S., García-Bordejé, E., Valverde, J.L., Romeo, E., and Monzón, A., 2013, A Langmuir–Hinshelwood approach to the kinetic modelling of catalytic ammonia decomposition in an integral reactor, *Phys. Chem. Chem. Phys.*, 15 (29), 12104–12117.

[33] Sauer, E., and Gross, J., 2019, Prediction of adsorption isotherms and selectivities: Comparison between classical density functional theory based on the perturbed-chain statistical associating fluid theory equation of state and ideal adsorbed solution theory, *Langmuir*, 35 (36), 11690–11701.

[34] Obaid, S.A., 2020, Langmuir, Freundlich, Tamkin, Adsorption isotherms and kinetics for the removal *Aartichoke tournefortii* straw from agricultural waste, *J. Phys.: Conf. Ser.*, 1664, 012011.

[35] Shiue, A., Ma, C.M., Ruan, R.T., and Chang, C.T., 2012, Adsorption kinetics and isotherms for the removal methyl orange from wastewaters using copper oxide catalyst prepared by the waste printed circuit boards, *Sustainable Environ. Res.*, 22 (4), 209–215.

[36] Qin, Q., Ma, J., and Liu, K., 2009, Adsorption of anionic dyes on ammonium-functionalized MCM-41, *J. Hazard. Mater.*, 162 (1), 133–139.

[37] Iida, Y., Kozuka, Tuziuti, T., and Yasui, K., 2004, Sonochemically enhanced adsorption and degradation of methyl orange with activated aluminas, *Ultrasonics*, 42 (1), 635–639.

[38] Wang, X., 2011, Preparation of magnetic hydroxyapatite and their use as recyclable adsorbent for phenol in wastewater, *Clean: Soil, Air, Water*, 39 (1), 13–20.

[39] Istratie, R., Stoia, M., Păcurariu, C., and Locovei, C., 2019, Single and simultaneous adsorption of methyl orange and phenol onto magnetic iron oxide/carbon nanocomposites, *Arabian J. Chem.*, 12 (8), 3704–3722.

[40] Luo, X., and Zhang, L., 2009, High effective adsorption of organic dyes on magnetic cellulose beads entrapping activated carbon, *J. Hazard. Mater.*, 171 (1-3), 340–347.

[41] Xie, Y., Qian, D., Wu, D., and Ma, X., 2011, Magnetic halloysite nanotubes/iron oxide composites for the adsorption of dyes, *Chem. Eng. J.*, 168 (2), 959–963.

[42] Wu, D., Zheng, P., Chang, P.R., and Ma, X., 2011, Preparation and characterization of magnetic rectorite/iron oxide nanocomposites and its application for the removal of the dyes, *Chem. Eng. J.*, 174 (1), 489–494.

[43] Zhu, H.Y., Jiang, R., Xiao, L., and Li, W., 2010, A novel magnetically separable γ-Fe_2O_3/cross-linked chitosan adsorbent: Preparation, characterization and adsorption application for removal of hazardous azo dye, *J. Hazard. Mater.*, 179, 251–257.

[44] Chowdhury, Z.Z., Zain, S.M., Khan, R.A., and Islam, M.S., 2012, Preparation and characterizations of activated carbon from kenaf fiber for equilibrium adsorption studies of copper from wastewater, *Korean J. Chem. Eng.*, 29 (9), 1187–1195.

[45] Jaycock, M.J., and Parfitt, G.D., 1981, *Chemistry of Interfaces*, Halstead Press, Ultimo, NSW, Australia.

[46] Wu, L, Zhang, G., and Lin, J., 2020, The physiochemical properties and adsorption characteristics of processed pomelo peel as a carrier for epigallocatechin-3-gallate, *Molecules*, 25 (18), 4249.